Interaction of uniform current with a circular cylinder submerged below an ice sheet

Z. F. Li [a], G. X. Wu [a,b,*] and Y. Y. Shi [c]

[a] School of Naval Architecture and Ocean Engineering, Jiangsu University of Science and Technology, Zhenjiang 212003, China

[b] Department of Mechanical Engineering, University College London, Torrington Place, London WC1E 7JE, UK

[c] College of Shipbuilding Engineering, Harbin Engineering University, Harbin 150001, China

Abstract

The problem of a uniform current passing through a circular cylinder submerged below an ice sheet is considered. The fluid flow is described by the linearized velocity potential theory, while the ice sheet is modeled through a thin elastic plate floating on the water surface. The Green function due to a source is first derived, which satisfies all the boundary conditions apart from that on the body surface. Through differentiating the Green function with respect to the source position, the multipoles are obtained. This allows the disturbed velocity potential to be constructed in the form of an infinite series with unknown coefficients which are obtained from the boundary condition. The result shows that there is a critical Froude number which depends on the physical properties of the ice sheet. Below this number there will be no flexural waves propagating to infinity and above this number there will be two waves, one on each side of the body. When the depth based Froude number is larger than 1, there will always be a wave at far upstream of the body. This is similar to those noticed in the related problem and is different from that in the free surface problem without ice sheet. Various results are provided, including the properties of the dispersion equation, resistance and lift, ice sheet deflection, and their physical features are discussed.

Keywords: ice sheet deflection; uniform current; circular cylinder; critical Froude number; resistance and lift

1. Introduction

There have been an increasing interest in making use of the new shipping route through the Arctic as well as the resource extraction. This makes it more imperative to achieve a better understanding of the nature of fluid/structure/ice interactions. In some cases, the ice may be

* Corresponding author. Permanent address: Department of Mechanical Engineering, University College London, Torrington Place, London WCIE 7JE, UK. Tel.: +44 20 7679 3870; fax: +44 20 7388 0180.
E-mail address: g.wu@ucl.ac.uk (G.X. Wu)

distributed in water in many small blocks/pieces, or in the form of a large iceberg. In other cases, the ice has a very large horizontal extent, which in many practical considerations can be treated as infinity. The present work considers a problem in the latter case, in which a body is submerged below an ice sheet of infinite extent and its interaction with an incoming current.

Generally, a large ice sheet can be modelled as a thin elastic plate, which has been verified through the field observations (Robin, 1963) and experiments (Squire et al., 1988). Together with the linearized velocity potential theory for fluid flow, a large volume of work has been undertaken for the interactions of surface gravity wave with the floating ice sheet in the context of geophysical science. Fox and Squire (1990) considered wave interaction with an ice sheet of semi-infinite extent, while Meylan and Squire (1994) studied an ice sheet of finite extent. For propagation of flexural gravity wave through the ice sheet with varying physical properties, part of the wave energy would be reflected. Squire and Dixon (2001b) considered diffraction problem by change of ice thickness, while Chung and Linton (2005) considered polynyas or free surface confined between ice sheets. Through applying the matched eigenfunction expansions (MEE) (Fox and Squire, 1990), Barrett and Squire (1996) solved the problem of wave propagation through ice sheet with a crack for finite water depth. Later, by using the Green function, Squire and Dixon (2000) obtained the solution for a similar problem in the infinite water depth, and then extended the solution procedure to the multiple cracks (Squire and Dixon, 2001a). The problem in Squire and Dixon (2000) was divided into the symmetric and anti-symmetric parts, which were solved by Evans and Porter (2003). Later, the same authors also derived the solutions for the wave interaction with multiple straight cracks of infinite length (Porter and Evans, 2006) and finite length (Porter and Evans, 2007).

For practical considerations in engineering, it is also important to include the structure into fluid/ice sheet interaction. Das and Mandal (2006) used the multipole expansion method (Ursell, 1949) and obtained the solution for wave interaction with a circular cylinder submerged below an ice sheet of infinite extent, while Liu and Li (2016) derived the solution for a semi-circular cylinder on the flat seabed. Li et al. (2017b) solved the problem for a circular cylinder undergoing large amplitude oscillations, in which the body surface boundary condition was satisfied on its exact position based on the procedure of Wu (1993), and therefore the nonlinear effect of the body motion was included. For the wave interaction with a cylinder submerged below the water surface covered by a semi-infinite ice sheet, Sturova (2014) derived the Green function in a series form based on the method of MEE. This procedure was then extended to solve the problem of wave interactions with a cylinder submerged below a polynya or an ice floe (Sturova, 2015b). The Green function for the case with the water surface covered by an ice floe could be also obtained through the Wiener-Hopf technique, as has been done by Tkacheva (2015). For a body floating on a polynya, Ren et al. (2016) studied the interaction of waves with a floating rectangle in a polynya and the analytical solution was obtained through MEE. It was found that compared with the free surface case the hydrodynamic coefficients were a highly oscillatory function of the wave frequency. By combining the eigenfunction expansions in the ice covered region and boundary integral equation in open water region, Li et al. (2018a) used the hybrid method and solved the problem numerically. Based on the wide spacing approximation, the problem could be also solved based on the solutions for floating body without the ice and for polynya without the body, and some explicit formulas could be derived to reveal mechanism of the oscillatory behaviours of the results, as has been done in Li et al. (2017a). For ice sheet with a crack, Sturova (2015a) solved the problem of the wave interactions with a submerged cylinder, through the method similar to that in Sturova (2014). Li et al. (2018c) derived the Green function for an ice sheet with a crack in an integral form. The multipoles were further derived through which the analytical solution for a circular cylinder was obtained. This procedure obtaining the Green function for a single crack was later extended to obtain the Green function for ice sheet with multiple cracks, and it was used to get the numerical solution for a submerged cylinder of arbitrary shape through the boundary element method (Li et al., 2018b).

In the work above, the incoming flow is a propagating wave and the problem is to find its diffraction, as well as the wave radiation by the oscillation of the body in response to the wave excitation. In this work, we shall consider the problem of uniform current passing through a circular cylinder submerged below an infinitely extended ice sheet. The problem will be steady instead of periodic as in the work mentioned above. This leads to a different boundary condition on the ice sheet and therefore the Green function and subsequently the multipoles have to be reconstructed. From the solution, the nature of the steady progressing wave away from the body can be established. In particular, a critical speed exists below which no wave will propagate to infinity, as in the related problem of a vehicle or pressure moving with constant speed on the ice sheet (Takizawa, 1985, 1988). For the linear free surface problem, it is well known that when the depth based Froude number is larger than 1, no wave will exist away from the body. However, for the ice sheet problem, wave will exist at far upstream under such a condition, which makes the current problem quite different. It may be noticed that there have already been some studies using singularities to model a submerged body moving below the ice sheet. Savin and Savin (2012) for example used a dipole to approximate a circular cylinder, while Sturova (2013) obtained the solution for a submerged sphere through the multipole expansions (Wu, 1995).

The rest of the paper is organized as follows. In section 2, the linearized velocity potential flow problem for the uniform current interaction with a cylinder submerged below the ice sheet of infinite extent is described. The corresponding Green function due to a single source is derived in section 3.1 through Fourier transform. In section 3.2, the multipoles are obtained through differentiating the Green function with respect to the source position, and through which the solution for the circular cylinder is written in a series expansion. Various numerical results are presented in section 4, and conclusions are drawn in section 5.

2. Mathematical Model

The interaction problem of a uniform current with a circular cylinder submerged below an ice sheet is considered, as sketched in figure 1. The homogeneous ice sheet of density ρ_i and thickness h floating on water of density ρ_w is assumed to be infinitely extended. To describe the ice deflection and fluid flow, a Cartesian coordinate system $O-xz$ is introduced, with the x-axis being on the calm water surface and opposite to the direction of the uniform current, and z-axis pointing vertically upwards. The water has finite depth at $z=-H$, and the centre of the circular cylinder with radius a is at (x_0, z_0).

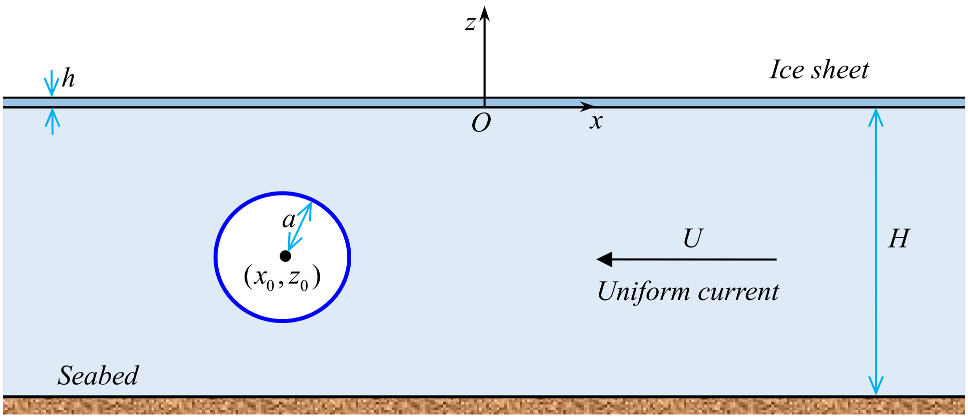

Fig. 1. Definition of the coordinate system and sketch of the problem.

Denoting η as the small vertical deflection of the ice sheet, then its flexural motion can be described through the well-established thin elastic plate model (Squire, 2011), or

$$(L\frac{\partial^4}{\partial x^4}+m\frac{\partial^2}{\partial t^2})\eta = p \quad (z=0), \tag{1}$$

where p is the pressure on the ice sheet, $L = Eh^3/[12(1-\nu^2)]$ and $m=\rho_i h$ are respectively the flexural rigidity and mass per unit area of the ice sheet, E is the Young's modulus, ν is Poisson's ratio. Following Squire (2011) which reviewed the work on wave/ice sheet interaction problems, the velocity potential theory is adopted to describe the fluid flow, i.e. the fluid is assumed to be inviscid, incompressible and homogeneous, and its motion to be irrotational. Also, the wave amplitude generated by the disturbance of the body is assumed to be small compared with the wavelength, i.e. all the boundary conditions are linearized. We may write the total velocity potential Φ as

$$\Phi = -U(x-\phi), \tag{2}$$

where ϕ is the disturbed velocity potential by the cylinder. The conservation of mass requires that ϕ should satisfy the Laplace equation

$$\nabla^2\phi \equiv \partial^2\phi/\partial x^2 + \partial^2\phi/\partial z^2 = 0, \tag{3}$$

throughout the fluid Ω. Assuming that there is no gap between the ice sheet S_I and the water upper surface, then the kinematic condition requires the fluid particle velocity in the normal direction of the ice sheet equal to that of the ice deflection, i.e.

$$(\frac{\partial}{\partial t} - U\frac{\partial}{\partial x})\eta = U\frac{\partial\phi}{\partial z} \quad (z=0), \tag{4}$$

where the higher order terms have been dropped. p in (1) should be the difference between the water pressure and atmospheric pressure. Through the Bernoulli's equation, we have

$$p = -\rho_w(\frac{\partial\Phi}{\partial t} + \frac{1}{2}\nabla\Phi\cdot\nabla\Phi + g\eta - \frac{1}{2}U^2) \quad (z=\eta). \tag{5}$$

where g is the acceleration due to gravity. Substituting (2) and (5) into (1), and ignoring the higher order terms, we have the dynamic condition at S_I as

$$(L\frac{\partial^4}{\partial x^4} + m\frac{\partial^2}{\partial t^2} + \rho_w g)\eta = -\rho_w U(\frac{\partial}{\partial t} - U\frac{\partial}{\partial x})\phi \quad (z=0). \tag{6}$$

We may combine the boundary conditions in (4) and (6), and obtain the boundary condition for ϕ as

$$(L\frac{\partial^4}{\partial x^4} + m\frac{\partial^2}{\partial t^2} + \rho_w g)\frac{\partial\phi}{\partial z} + \rho_w(\frac{\partial}{\partial t} - U\frac{\partial}{\partial x})^2\phi = 0 \quad (z=0). \tag{7}$$

Here, when the problem becomes steady in the uniform current, the temporal derivatives of both ϕ and η should be equal to zero. Equation (7) can be further given as

$$(L\frac{\partial^4}{\partial x^4} + \rho_w g)\frac{\partial\phi}{\partial z} + \rho_w U^2\frac{\partial^2\phi}{\partial x^2} = 0 \quad (z=0). \tag{8}$$

It may be noticed that (8) is different from that in Squire et al. (1996) by a term of $mU^2\partial^3\phi/\partial z\partial x^2$. In fact, they considered the problem of a load moving with constant speed U on the ice sheet. It was solved in the system moving with the load, or the load was not moving but the ice sheet and water were moving with speed U. As a result, due to the curvature of the ice sheet, its horizontal speed created a vertical acceleration $U^2\partial^2\eta/\partial x^2$, which led to an additional term $mU^2\partial^3\phi/\partial z\partial x^2$ in (8). Here, the cylinder is stationary and so is the ice sheet, and only the water is moving towards cylinder with speed U. Therefore this term does not appear. For the steady problem, (4) becomes

$$\frac{\partial \phi}{\partial z}+\frac{\partial \eta}{\partial x}=0 \quad (z=0), \tag{9}$$

and (6) provides

$$\eta=\frac{1}{\rho_w g}(-L\frac{\partial^4 \eta}{\partial x^4}+\rho_w U^2\frac{\partial \phi}{\partial x}) \quad (z=0), \tag{10}$$

or with (9) considered

$$\eta=\frac{1}{\rho_w g}(L\frac{\partial^4 \phi}{\partial z \partial x^3}+\rho_w U^2\frac{\partial \phi}{\partial x}) \quad (z=0). \tag{11}$$

On the body surface S_H, the impermeable condition can be written as

$$\frac{\partial \phi}{\partial n}=n_x, \tag{12}$$

where $\vec{n}=(n_x, n_z)$ is the unit normal vector pointing out of the fluid domain. Similarly, on the flat seabed S_B, the impermeable condition gives

$$\frac{\partial \phi}{\partial z}=0 \quad (-\infty<x<+\infty, \; z=-H). \tag{13}$$

The radiation condition far away from the body can be expressed as

$$\frac{\partial \phi}{\partial x}=w_{\pm}(x,z) \quad \text{as} \quad x\rightarrow \pm\infty, \tag{14}$$

where $w_{\pm}(x,z)$ correspond to the wavy functions oscillating with x at $x\rightarrow\pm\infty$ respectively, depending on whether the group velocity of the wave is larger or smaller than the current speed U.

3. Solution Procedures

3.1. The Green function

The Green function $G(x,z;x_0,z_0)$ represents the velocity potential at the field point $p(x,y)$ due to a source at point $q(x_0,z_0)$. This means that it should satisfy the following governing equation

$$\nabla^2 G=2\pi\delta(x-x_0)\delta(z-z_0), \tag{15}$$

together with the boundary conditions in (8), (13) and (14). Here, $\delta(x)$ is the Dirac delta function. Applying the Fourier transform

$$\tilde{G}=\frac{1}{2\pi}\int_{-\infty}^{+\infty}G\mathrm{e}^{-\mathrm{i}kx}\mathrm{d}x, \tag{16}$$

to (15), we have

$$-k^2\tilde{G}(k,z)+\frac{\partial^2\tilde{G}(k,z)}{\partial z^2}=\delta(z-z_0)\mathrm{e}^{-\mathrm{i}kx_0}. \tag{17}$$

The solution to (17) together with the boundary condition in (13) can be written as

$$\tilde{G}=\frac{\mathrm{e}^{-\mathrm{i}kx_0}}{k}[\alpha k\cosh(kz_>)+\beta\sinh(kz_>)]Z(z_<,k)\,, \tag{18}$$

where α and β are two unknown functions of k to be found, $z_>=\max(z,z_0)$, $z_<=\min(z,z_0)$, and

$$Z(z,k)=\cosh[k(z+H)]\,. \tag{19}$$

Integrating (17) with respect to z from z_0^- to z_0^+, then substituting (18) into the obtained result, we have

$$-\alpha k\sinh(kH)+\beta\cosh(kH)=1\,. \tag{20}$$

We then apply the Fourier transform to the boundary condition in (8) on the ice sheet, and have

$$(Lk^4+\rho_w g)\frac{\partial\tilde{G}}{\partial z}-\rho_w U^2k^2\tilde{G}=0\,. \tag{21}$$

Substituting (18) into (21), and invoking (20), we have

$$\alpha=-\frac{Lk^4+\rho_w g}{K(U,k)Z(0,k)}\quad\text{and}\quad\beta=-\frac{\rho_w U^2k^2}{K(U,k)Z(0,k)}\,, \tag{22}$$

where

$$K(U,k)=(Lk^4+\rho_w g)k\tanh(kH)-\rho_w U^2k^2\,. \tag{23}$$

Substituting (22) into (18), we have

$$\tilde{G}=-\frac{\mathrm{e}^{-\mathrm{i}kx_0}}{k}\frac{(Lk^4+\rho_w g)k\cosh(kz_>)+\rho_w U^2k^2\sinh(kz_>)}{K(U,k)Z(0,k)}Z(z_<,k)\,. \tag{24}$$

Performing the inverse Fourier transform

$$G=\int_{-\infty}^{+\infty}\tilde{G}\mathrm{e}^{+\mathrm{i}kx}\mathrm{d}k\,, \tag{25}$$

to (24), and using

$$\ln(\frac{r_1}{H})=\int_0^{+\infty}\frac{\mathrm{e}^{-kH}-\mathrm{e}^{-k(z_>-z_<)}\cos[k(x-x_0)]}{k}\mathrm{d}k\,, \tag{26}$$

$$\ln(\frac{r_2}{H})=\int_0^{+\infty}\frac{\mathrm{e}^{-kH}-\mathrm{e}^{-k(z_>+z_<+2H)}\cos[k(x-x_0)]}{k}\mathrm{d}k\,, \tag{27}$$

with r_1 as the distance between p and q, and r_2 as the distance between p and the mirror image of q about the flat seabed $z=-H$, we can obtain

$$G=\ln(\frac{r_1}{H})+\ln(\frac{r_2}{H})+2\int_0^{+\infty}\frac{\mathrm{e}^{-kH}}{k}\frac{P(U,k)}{K(U,k)}\frac{Z(z_0,k)}{Z(0,k)}\{1-Z(z,k)\cos[k(x-x_0)]\}\mathrm{d}k\,, \tag{28}$$

where

$$P(U,k)=(Lk^4+\rho_w g)k+\rho_w U^2k^2\,, \tag{29}$$

It ought to be pointed out that a constant has been added into the integrand of (28) to remove the high order singularity at $k=0$. This will not affect the physics of the problem as the equations for

G all involve spatial derivatives.

We notice that when $h \to 0$ or $L \to 0$, G in (28) will become equation (13.46) of Wehausen and Laitone (1960) for free surface. We further notice that the integrand in (28) is singular at $K(U,k_m)=0$, where $m=1,\ldots,M$ include all the positive real roots. Here, M could be 0, 1 or 2 depending on the Froude number, which will be discussed later. The way to deal with the singularities will be based on the radiation condition. To do that, we may use (Wehausen and Laitone, 1960)

$$\lim_{R\to+\infty}\int_{k_a}^{k_b}\frac{f(k)}{k-k_0}\mathrm{e}^{\pm \mathrm{i}R(k-k_0)}\mathrm{d}k=\pm\mathrm{i}\pi f(k_0), \tag{30}$$

where the integral is in Cauchy principle value integration sense, and $k_a<k_0<k_b$. To satisfy the radiation condition in (14), we add the minus or plus term of the integration at $x\to\pm\infty$ accordingly. Thus we have

$$\begin{aligned}G=&\ln(\frac{r_1}{H})+\ln(\frac{r_2}{H})+2\int_0^{+\infty}\frac{\mathrm{e}^{-kH}}{k}\frac{P(U,k)}{K(U,k)}\frac{Z(z_0,k)}{Z(0,k)}\{1-Z(z,k)\cos[k(x-x_0)]\}\mathrm{d}k\\&-2\pi\sum_{m=1}^{M}\chi_m\frac{\mathrm{e}^{-k_mH}}{k_m}\frac{P(U,k_m)}{K^{(1)}(U,k_m)}\frac{Z(z_0,k_m)}{Z(0,k_m)}Z(z,k_m)\sin[k_m(x-x_0)]\end{aligned}, \tag{31}$$

where $\chi_m=+1$ ($\chi_m=-1$) if the group velocity of the wave component of k_m is smaller (larger) than U, and the superscript (n) in $K(U,k)$ indicates the n-th partial derivative with respect to the variable k. It should be noticed that the integral in (31) is in Cauchy principle value integration sense.

3.2. Multipole expansion for a submerged circular cylinder

We may obtain the velocity potential due to multipoles or singularity of higher orders by differentiating (31) with respect to the source position. Thus, the boundary conditions satisfied by G will be still satisfied. Similar to Wu (1998), we have

$$(D_\pm)^n\ln(r_1)=\frac{\mathrm{e}^{\pm\mathrm{i}n\theta}}{r^n}, \tag{32}$$

where $x-x_0=r\sin\theta$, $z-z_0=r\cos\theta$, and the operator $(D_\pm)^n$ is defined as

$$(D_\pm)^n=-\frac{1}{2^{n-1}(n-1)!}(\frac{\partial}{\partial z_0}\pm\mathrm{i}\frac{\partial}{\partial x_0})^n. \tag{33}$$

As G is a real function, $(D_+)^n$ and $(D_-)^n$ will lead to a pair of conjugates. Applying (33) to (31), and noticing that $(D_+)\exp(\pm kz_0\pm\mathrm{i}kx_0)=0$ and $(D_-)\exp(\pm kz_0\mp\mathrm{i}kx_0)=0$, we have

$$
\begin{aligned}
f_n = (D_+)^n G = \frac{\mathrm{e}^{+\mathrm{i}n\theta}}{r^n} + \frac{(-1)^n}{(n-1)!}\int_0^{+\infty} k^{n-1}\mathrm{e}^{-k(z+z_0+2H)-\mathrm{i}k(x-x_0)}\mathrm{d}k - f_{c1}(z_0,n) \\
+\frac{1}{(n-1)!}\int_0^{+\infty}\frac{P(U,k)}{K(U,k)}\frac{Z(z,k)}{Z(0,k)}k^{n-1}[\mathrm{e}^{+kz_0+\mathrm{i}k(x-x_0)}+(-1)^n\mathrm{e}^{-k(z_0+2H)-\mathrm{i}k(x-x_0)}]\mathrm{d}k \\
-\frac{\mathrm{i}\pi}{(n-1)!}\sum_{m=1}^{M}\frac{\chi_m P(U,k_m)}{K^{(1)}(U,k_m)}\frac{Z(z,k_m)}{Z(0,k_m)}k_m^{n-1}[\mathrm{e}^{+k_m z_0+\mathrm{i}k_m(x-x_0)}-(-1)^n\mathrm{e}^{-k_m(z_0+2H)-\mathrm{i}k_m(x-x_0)}]
\end{aligned}
\quad , \tag{34}
$$

where

$$
f_{c1}(z_0,n) = \frac{1}{(n-1)!}\int_0^{+\infty}\frac{P(U,k)}{K(U,k)}\frac{k^{n-1}}{Z(0,k)}\frac{\mathrm{e}^{+kz_0}+(-1)^n\mathrm{e}^{-k(z_0+2H)}}{2^{n-1}}\mathrm{d}k\,. \tag{35}
$$

Using equation (34), we can write the disturbed velocity potential ϕ in form of multipole expansion as

$$
\phi = \mathrm{Re}(\sum_{n=1}^{\infty} a^n A_n f_n)\,. \tag{36}
$$

Then ϕ satisfies the same boundary conditions as f_n automatically, or satisfies all the boundary conditions apart from that on the body surface, which are to be used to determine the unknown coefficients A_n. Substituting (36) into (12), we have

$$
\frac{\partial\phi}{\partial r} = -\frac{\partial\phi}{\partial n} = \mathrm{Re}(\frac{\mathrm{e}^{+\mathrm{i}\theta}}{\mathrm{i}}) \quad (r=a). \tag{37}
$$

We may use

$$
\mathrm{e}^{kz\pm\mathrm{i}kx} = \mathrm{e}^{kz_0\pm\mathrm{i}kx_0}\sum_{l=0}^{\infty}\frac{k^l r^l\mathrm{e}^{\pm\mathrm{i}l\theta}}{l!} \quad\text{and}\quad \mathrm{e}^{-kz\pm\mathrm{i}kx} = \mathrm{e}^{-kz_0\pm\mathrm{i}kx_0}\sum_{l=0}^{\infty}\frac{(-1)^l k^l r^l\mathrm{e}^{\mp\mathrm{i}l\theta}}{l!}\,, \tag{38}
$$

to write ϕ in the polar coordinate system as

$$
\phi = \mathrm{Re}\{\sum_{n=1}^{\infty}A_n a^n\{\frac{\mathrm{e}^{+\mathrm{i}n\theta}}{r^n}+\frac{1}{(n-1)!}\sum_{l=0}^{\infty}\frac{r^l}{l!}[\mathrm{e}^{+\mathrm{i}l\theta}J_1(n,l)+\mathrm{e}^{-\mathrm{i}l\theta}J_2(n,l)]-f_{c1}(z_0,n)\}\}\,, \tag{39}
$$

where

$$
J_1(n,l) = (-1)^{n+l}F_1(n+l)+F_2(n+l) \quad\text{and}\quad J_2(n,l)=(-1)^l F_3(n+l)\,, \tag{40}
$$

with

$$
F_1(n) = \int_0^{+\infty}k^{n-1}\mathrm{e}^{-2k(z_0+H)}\mathrm{d}k = \frac{(n-1)!}{[2(z_0+H)]^n}\,, \tag{41}
$$

$$
\begin{aligned}
F_2(n) = \int_0^{+\infty}\frac{P(U,k)}{2K(U,k)}\frac{\mathrm{e}^{-kH}}{Z(0,k)}k^{n-1}[\mathrm{e}^{+2k(z_0+H)}+(-1)^n\mathrm{e}^{-2k(z_0+H)}]\mathrm{d}k \\
-\mathrm{i}\pi\sum_{m=1}^{M}\frac{\chi_m P(U,k_m)}{2K^{(1)}(U,k_m)}\frac{\mathrm{e}^{-k_m H}}{Z(0,k_m)}k_m^{n-1}[\mathrm{e}^{+2k_m(z_0+H)}-(-1)^n\mathrm{e}^{-2k_m(z_0+H)}]
\end{aligned}
\,, \tag{42}
$$

$$
\begin{aligned}
F_3(n) = \int_0^{+\infty}\frac{P(U,k)}{2K(U,k)}\frac{\mathrm{e}^{-kH}}{Z(0,k)}k^{n-1}[1+(-1)^n]\mathrm{d}k \\
-\mathrm{i}\pi\sum_{m=1}^{M}\frac{\chi_m P(U,k_m)}{2K^{(1)}(U,k_m)}\frac{\mathrm{e}^{-k_m H}}{Z(0,k_m)}k_m^{n-1}[1-(-1)^n]
\end{aligned}
\,. \tag{43}
$$

Invoking (37) and the orthogonality of trigonometric function, we can obtain

$$-l\frac{A_l}{a}+\sum_{n=1}^{\infty}\frac{A_n a^{n+l-1}J_1(n,l)}{(n-1)!(l-1)!}+\sum_{n=1}^{\infty}\frac{\overline{A}_n a^{n+l-1}\overline{J}_2(n,l)}{(n-1)!(l-1)!}=\frac{\delta_{l1}}{\mathrm{i}}\,, \tag{44}$$

for $l=1,2,\ldots$, where δ_{l1} is the Kronecker delta function. This equation can be solved by separating the real and imaginary parts, or by taking the conjugate and obtaining another set of equations.

After the disturbed velocity potential ϕ is solved, we can obtain the hydrodynamic pressure in the fluid domain through the Bernoulli equation (5) or

$$p=-\frac{1}{2}\rho_w U^2[\nabla(\phi-x)\cdot\nabla(\phi-x)-1]\,. \tag{45}$$

Here, it may be noticed that by following the argument of Wu (1991), although the higher order terms can be ignored in the upper surface condition, they may be retained near the body surface as the local disturbance may not be small. The resistance F_R and lift F_L of the cylinder can be obtained through integrating the pressure over the cylinder surface or

$$-\mathrm{i}\times F_R+F_L=-a\int_{-\pi}^{+\pi}(p\mathrm{e}^{\mathrm{i}\theta})_{r=a}\mathrm{d}\theta\,, \tag{46}$$

The gradient in (45) can be taken in the polar coordinate system. From the boundary condition on the body surface, we have

$$[\frac{\partial(\phi-x)}{\partial r}]_{r=a}=0\,. \tag{47}$$

Equation (39) provides

$$[\frac{\partial(\phi-x)}{\partial\theta}]_{r=a}=\mathrm{Re}\{\mathrm{i}\sum_{n=1}^{\infty}A_n\{n\mathrm{e}^{+\mathrm{i}n\theta}+\frac{1}{(n-1)!}\sum_{l=1}^{\infty}\frac{a^{n+l}}{(l-1)!}[\mathrm{e}^{+\mathrm{i}l\theta}J_1(n,l)-\mathrm{e}^{-\mathrm{i}l\theta}J_2(n,l)]\}\}-a\cos\theta\,. \tag{48}$$

Similar to Wu and Eatock Taylor (1987a), substituting (44) into (48) we have

$$[\frac{\partial(\phi-x)}{\partial\theta}]_{r=a}=-2\,\mathrm{Im}(\sum_{n=1}^{\infty}nA_n\mathrm{e}^{+\mathrm{i}n\theta})\,. \tag{49}$$

Substituting (47) and (49) into (45), then the results into (46), and noticing that

$$\mathrm{Im}(Z)\,\mathrm{Im}(Z)=-\frac{Z^2+\overline{Z}^2-2Z\overline{Z}}{4}\,, \tag{50}$$

we can obtain

$$-\mathrm{i}\times F_R+F_L=\frac{2\pi\rho_w U^2}{a}\sum_{n=1}^{\infty}n(n+1)A_n\overline{A}_{n+1}\,. \tag{51}$$

Through (11) we can also obtain the ice deflection η. By using

$$\frac{\mathrm{e}^{+\mathrm{i}n\theta}}{r^n}=\frac{1}{(n-1)!}\int_0^{+\infty}k^{n-1}\mathrm{e}^{-k(z-z_0)+\mathrm{i}k(x-x_0)}\mathrm{d}k\,, \tag{52}$$

we have

$$\eta = -\frac{1}{\rho_w g}\mathrm{Im}\{\sum_{n=1}^{\infty}\frac{a^n A_n}{(n-1)!}[G_1(n) - G_2(n)]\} . \tag{53}$$

where

$$\begin{aligned} G_1(n) = L\{&\frac{(n+3)!}{[(-z_0)-\mathrm{i}(x-x_0)]^{n+4}} - (-1)^n \frac{(n+3)!}{[(2H+z_0)+\mathrm{i}(x-x_0)]^{n+4}}\} \\ + \rho_w U^2 \{&\frac{n!}{[(-z_0)-\mathrm{i}(x-x_0)]^{n+1}} - (-1)^n \frac{n!}{[(2H+z_0)+\mathrm{i}(x-x_0)]^{n+1}}\} \end{aligned} , \tag{54}$$

$$\begin{aligned} G_2(n) = &\int_0^{+\infty}\frac{P(U,k)}{K(U,k)}k^n[Lk^3\tanh(kH) - \rho_w U^2][\mathrm{e}^{+kz_0+\mathrm{i}k(x-x_0)} - (-1)^n \mathrm{e}^{-k(z_0+2H)-\mathrm{i}k(x-x_0)}]\mathrm{d}k \\ &- i\pi\sum_{m=1}^{M}\frac{\chi_m P(U,k_m)}{K^{(1)}(U,k_m)}k_m^n[Lk_m^3\tanh(k_m H) - \rho_w U^2][\mathrm{e}^{+k_m z_0+\mathrm{i}k_m(x-x_0)} + (-1)^n \mathrm{e}^{-k_m(z_0+2H)-\mathrm{i}k_m(x-x_0)}]\} \end{aligned} . \tag{55}$$

4. Numerical Results

The typical values of the parameters of the ice sheet are given as (Sturova, 2015b)

$$E = 5\mathrm{GPa}\ ,\ \ \nu = 0.3\ ,\ \ \rho_i = 922.5\mathrm{kg/m^3}\ ,\ \ h = 1\mathrm{m}\ . \tag{56}$$

Unless otherwise stated, the calculations will be carried out with the parameters given in (56). In the following text, all the numerical results are provided in the dimensionless form, based on the combinations of the radius of the cylinder a, density of water $\rho_w = 1025\mathrm{kg/m^3}$, and acceleration due to gravity $g = 9.80\mathrm{m/s^2}$.

4.1. Properties of the purely positive real root of the dispersion equation

From the expression of the Green function G in (31), we can see that the wave due to a single source will be very much related to the purely positive real root of the dispersion equation. To carry out analysis, we may rewrite $K(U,k) = 0$ as

$$\frac{\tanh(\hat{k})}{\hat{k}} = \frac{Fn^2}{D\hat{k}^4 + 1}, \tag{57}$$

where $\hat{k} = kH$, $D = L/(\rho_w g H^4)$, and $Fn = U/\sqrt{gH}$ is the water depth Froude number. We may denote the left and right hand sides of (57) respectively by $L_d(\hat{k})$ and $R_d(\hat{k})$. We notice that $R_d(\hat{k})$ decays much faster than $L_d(\hat{k})$ as $\hat{k} \to +\infty$. This means at sufficiently large $\hat{k}$, $R_d(\hat{k}) < L_d(\hat{k})$. Thus, when there exists a $\hat{k}_0$ at which $R_d(\hat{k}_0) > L_d(\hat{k}_0)$, equation (57) will definitely have at least one solution. For this reason, we let $\hat{k}_0 = 0$ in (57). In such a case when $Fn \geq 1$, the equation will always have at least one solution. For $Fn < 1$, equation (57) should have either at least two solutions, which means that $L_d(\hat{k})$ and $R_d(\hat{k})$ intersect twice, or no solution, which means they do not intersect. A special case of the former is that the two solutions merge into one, and $L_d(\hat{k})$ and $R_d(\hat{k})$ are tangential to each other when they intersect. This is shown graphically in figure 2. From the figure, it can be seen that there is a critical Froude number

Fn_c, below which equation (57) will have no solution or there will be no waves at $x = \pm\infty$. At $Fn = Fn_c$, $L_d(\hat{k})$ and $R_d(\hat{k})$ should satisfy equation (57) and at the same point their derivatives should be the same, or

$$\frac{\hat{k}\,\mathrm{sech}^2(\hat{k}) - \tanh(\hat{k})}{\hat{k}^2} = -\frac{4D\hat{k}^3 Fn^2}{(D\hat{k}^4+1)^2}. \tag{58}$$

Invoking (57), we may rewrite (58) as

$$D^2\hat{k}^8 + D(2+3Fn^2)\hat{k}^4 - Fn^4\hat{k}^2 + (1-Fn^2) = 0. \tag{59}$$

Equations (57) and (59) can be solved through the Newton iteration method, to obtain Fn_c and the associated wave number $\hat{k}_c$, which provides $Fn_c = 0.7869$ and $\hat{k}_c = 1.9707$ for the parameters given in (56). The variation of the root $\hat{k}_m$ ($m = 1, 2$) with respect to the Froude number Fn can be more clearly seen in figure 3 which plots $\hat{k}_m$ together with the result for $h = 0$ corresponding to the free surface.

In order to determine the sign of χ_m in (31), we should compute the group velocity of the wave component for $\hat{k}_m$, or

$$\begin{aligned} c_g(Fn,\hat{k}_m) &= Fn + \hat{k}_m \frac{\mathrm{d}Fn}{\mathrm{d}\hat{k}_m} \\ &= Fn + \hat{k}_m \frac{D\hat{k}_m^4+1}{2Fn}\left[\frac{\hat{k}_m\,\mathrm{sech}^2(\hat{k}_m) - \tanh(\hat{k}_m)}{\hat{k}_m^2} + \frac{4D\hat{k}_m^3 Fn^2}{(D\hat{k}_m^4+1)^2}\right]. \end{aligned} \tag{60}$$

The term in square brackets of (60) corresponds to (58). This indicates that when it is negative (positive) at $\hat{k}_m < \hat{k}_c$ ($\hat{k}_m > \hat{k}_c$), the group velocity $c_g(Fn,\hat{k}_m) < Fn$ ($c_g(Fn,\hat{k}_m) > Fn$), we should have $\chi_m = +1$ ($\chi_m = -1$) and the wave of $\hat{k}_m$ will be at $x = -\infty$ ($x = +\infty$) respectively. This is the case when $Fn_c < Fn < 1$. At $Fn < Fn_c$, there will be no wave propagating to the far field, or only when the speed is larger than a critical value, far field wave can be generated. As in the cases discussed by Takizawa (1988) and Squire et al. (1996) for a moving load on an infinitely extended ice sheet, a critical speed exists, below which there will be no propagating wave, while above which wave may exist both upstream and downstream, depending on its group velocity.

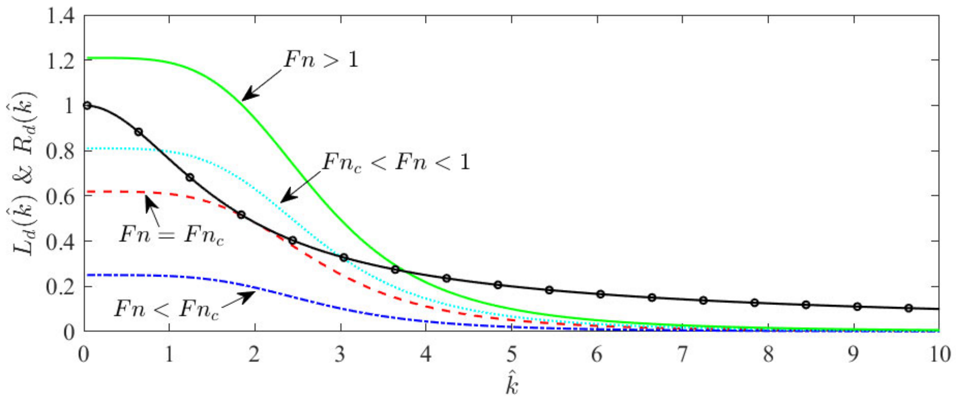

Fig. 2. Curves for $L_d(\hat{k})$ and $R_d(\hat{k})$ in equation (57) against $\hat{k}$, at different Froude number Fn. Solid line: $R_d(\hat{k})$ with $Fn=1.1$; dashed line: $R_d(\hat{k})$ with $Fn=Fn_c=0.7869$; dash-dotted line: $R_d(\hat{k})$ with $Fn=0.5$; dotted line: $R_d(\hat{k})$ with $Fn=0.9$; solid line with open circles: $L_d(\hat{k})$. ($a=1$, $H=8$, $h=0.2$, $L=72.9319$)

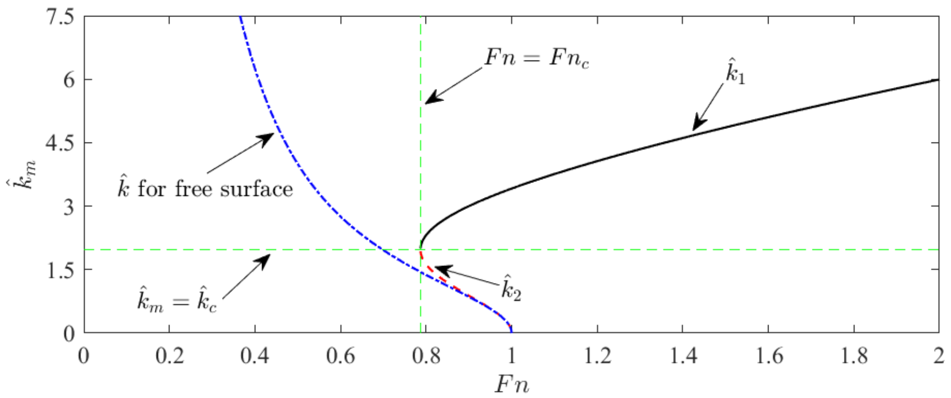

Fig. 3. Purely positive real root $\hat{k}_m$ of the dispersion equation $K(U,k)=0$ against Fn. Solid line: $\hat{k}_1$ ($c_g \geq Fn$); dashed line: $\hat{k}_2$ ($c_g \leq Fn$); dash-dotted line: $\hat{k}$ for open water. ($a=1$, $H=8$, $h=0.2$, $L=72.9319$)

4.2. Resistance and lift

We consider the interaction problem of the uniform current with a circular cylinder submerged below the ice sheet. To conduct numerical computations, the infinite summation in (44) is truncated at a finite number or $n=N$. Convergence study is first carried out with respect to N through the resistance F_R and lift F_L against the Froude number Fn. The computed results are shown in figure 4, together with the results for open water or $h=0$. It can be seen from the figure that there is no visible difference between the results obtained by $N=6$ and $N=12$, indicating that the convergence has been achieved. Therefore, in the following computed results $N=6$ is taken, unless otherwise specified. From figure 4 (*a*) we can see that when $Fn<Fn_c$, F_R is zero, and there is no wave far away from the body as there is no purely positive real root of the dispersion equation or $M=0$ in (31). From the formulation in section 3, when $M=0$, the functions $F_1(n)$, $F_2(n)$ and $F_3(n)$ in (41) to (43) are all real, which means that $J_1(n,l)$ and $J_2(n,l)$ in (40) are both real. This together with (44) indicates that all A_n are imaginary numbers or the right hand side of (51) is a real number, leading to $F_R=0$. However, F_L is still nonzero. For the open water case, $Fn=1$ is the critical Froude number. Beyond this $F_R=0$, which is well known for the linearized free surface problem.

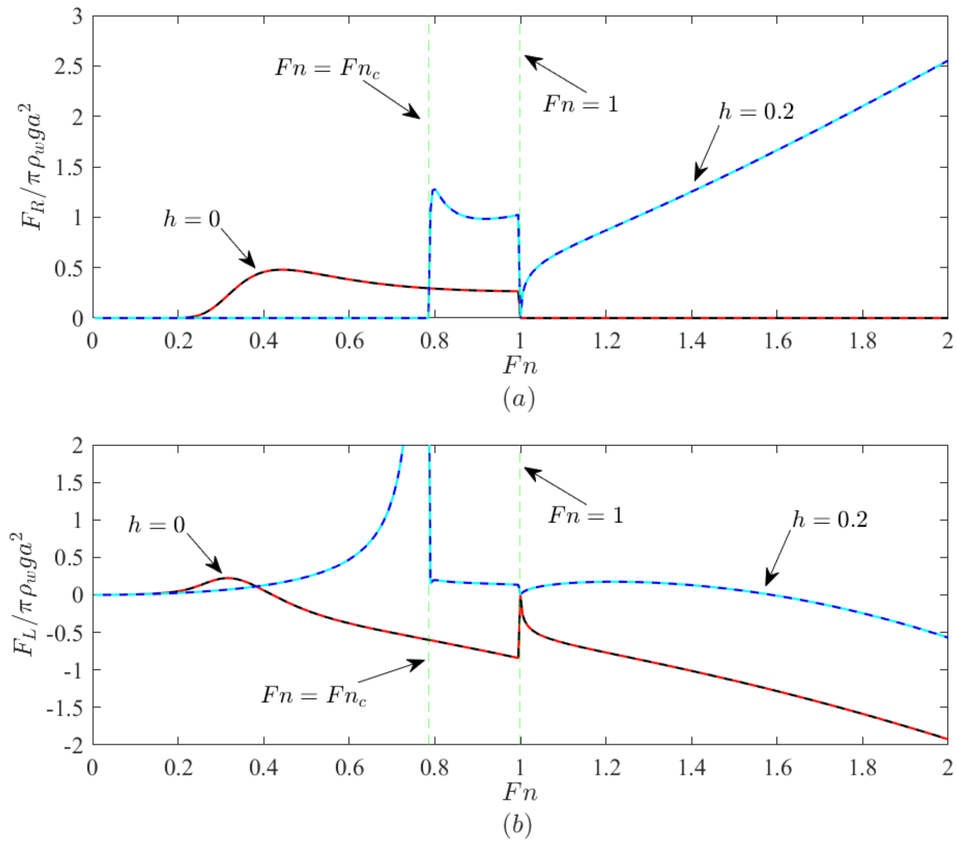

Fig. 4. Resistance (*a*) and lift (*b*) of a circular cylinder submerged below an ice sheet against Fn at different N. Solid lines: results with $N=6$; dashed lines: results with $N=12$. ($a=1$, $(x_0,z_0)=(0,-2)$, $H=8$, $h=0.2$, $L=72.9319$)

In figure 5, we show the variations of the resistance and lift against Fn at five different ice thicknesses h, i.e. $h=0$, 0.002, 0.02, 0.1 and 0.2. It can be seen from this figure that when the ice thickness tends to zero or $h\to 0$, the result for ice sheet will tend to that for open water, as reflected by the result for $h=0.002$ marked by the open circles. This is not unexpected. From (8) we have that when $h\to 0$ or $L=O(h^3)\to 0$, the condition on the ice sheet will tend to that for open water, and the same boundary conditions will lead to the same results. At the same time $Fn_c\to 0$. As the ice thickness h increases, the difference between the results with ice sheet and those for open water becomes obvious. For the resistance, from figure 5 (*a*), we can see that there are two critical values of Fn at which a sudden change of F_R will happen. These two critical points are respectively at the critical Froude number or $Fn=Fn_c$ and $Fn=1$, at which there will be a sudden change of the wave system in the far field, or the number of wave components in the far field will change from 0 to 2 in the former, and from 2 to 1 in the latter. Also, it can be seen from figure 5 (*a*) that when $Fn>Fn_c$, the resistance with the ice sheet is generally larger than that for open water, and it increases with the ice thickness h. Another feature of the resistance with ice sheet is that unlike the open water case, even when $Fn>1$, F_R is not zero, due to the fact that there is always a wave in front of the cylinder. As Fn increases,

F_R increases. However, it is not expected to continue when Fn is sufficiently large. In fact from (57), we have $\hat{k} \approx (Fn^2 / D)^{1/3}$ at very large Fn. As $\hat{k} \to +\infty$, the imaginary part of both $F_2(n)$ and $F_3(n)$ will tend to zero, and therefore the resistance will eventually tend to zero as $Fn \to +\infty$. For the lift F_L, it can be seen from figure 5 (*b*) that F_L will first increase with Fn. It will reach a large peak before $Fn = Fn_c$, e.g. respectively at $Fn = 0.335$, 0.605, 0.775 for $h = 0.02$, 0.10, 0.20 with $Fn_c = 0.3376$, 0.6168, 0.7869, and then drop rapidly and become mainly negative. It is interesting to see here that the peak happens before Fn_c not at Fn_c. This is similar to the problem of a body advancing at forward speed U in a free surface wave with frequency ω. There is a critical point at $\tau = U\omega / g = 1/4$. However, the peak of the hydrodynamic coefficient occurs before $\tau = 1/4$ (Grue and Palm, 1985; Wu and Eatock Taylor, 1987b). At $\tau = 1/4$, the results are finite (Mo and Palm, 1987). As Fn further increases it will have a jump at $Fn = 1$, but remain negative.

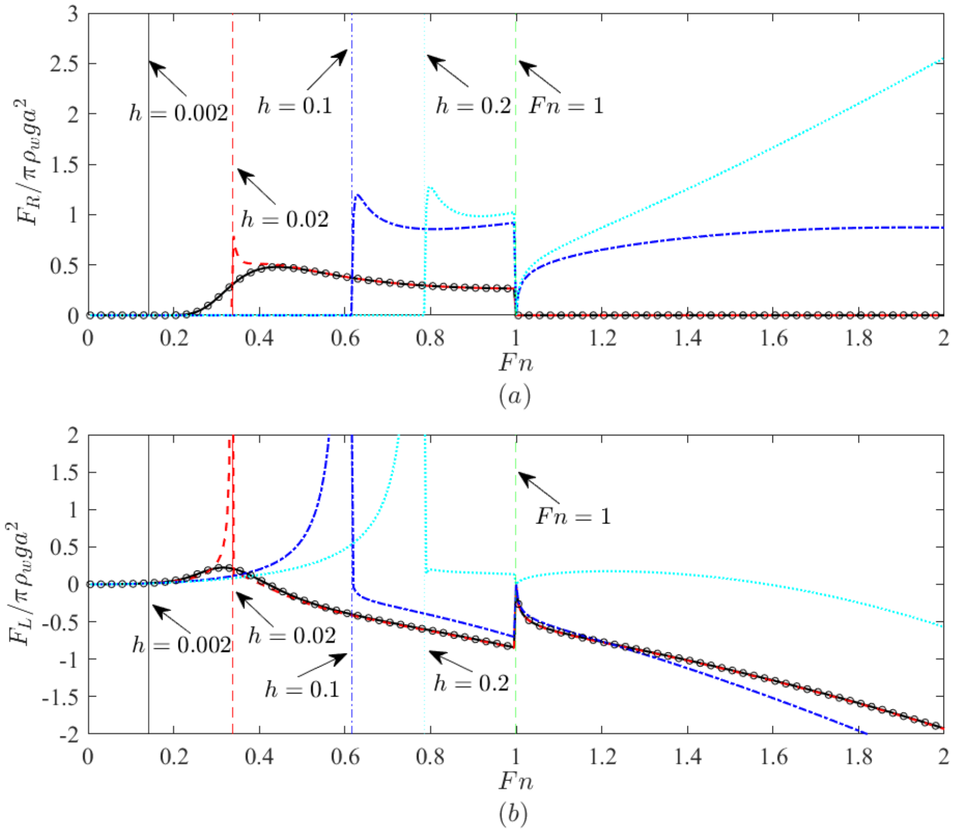

Fig. 5. Resistance (*a*) and lift (*b*) of a circular cylinder submerged below an ice sheet at different ice thickness h. Solid lines: $h = 0.002$; dashed lines: $h = 0.02$; dash-dotted lines: $h = 0.1$; dotted lines: $h = 0.2$; open circles: $h = 0$. ($a = 1$, $(x_0, z_0) = (0, -2)$, $H = 8$, $L = 72.9319$)

Computations are then carried out to investigate the effect of the water depth H. For infinite water depth or $H \to +\infty$, the dispersion equation (23) provides

$$Lk^4 + \rho_w g = \rho_w U^2 k \, . \tag{61}$$

Similar to the finite water depth, there exists a critical speed U_c, below which no waves will exist at the far field. At $U = U_c$, the right hand side and left hand side of (61) should be tangential to each other, or

$$4Lk_c^3 = \rho_w U_c^2 . \tag{62}$$

This together with (61) provides that

$$U_c = (\frac{256Lg^3}{27\rho_w})^{1/8} \text{ and } k_c = (\frac{\rho_w g}{3L})^{1/4}, \tag{63}$$

which is consistent with (5.5) of Squire et al. (1996). If we use the wavelength $2\pi / k_c$ as the length scale, the critical Froude number will be $\tilde{Fn}_c = \sqrt{2/3\pi}$. When $U > U_c$ there will be two purely positive real roots k_1 and k_2 of (61), while when $U < U_c$ there will be no root. It should be noted that k_1 and k_2 will always exist, unlike the finite what depth where k_2 disappears when the depth based Froude number is larger than 1.

In figure 6, we show the resistance and lift against the body submergence based Froude number $\tilde{Fn} = U/\sqrt{-gz_0}$ at three different H, i.e. $H = 8$, 12 and 16 together with infinite water depth. It can be seen from this figure that the effect of H on submergence based $\tilde{Fn}_c$ is small overall and the jump of the result occurs almost at the same location. In fact, when $k_c H$ is relatively large, where k_c is from (63), $\tanh(k_c H) \approx 1$ may be used. Thus $\tilde{Fn}_c$ can be obtained from the U_c in (63) with infinite water depth. However, the jump at depth based $Fn = 1$ occurs at different submergence based $\tilde{Fn}$ as shown in the figure, and this $\tilde{Fn}$ increases with H and tends to infinity as $H \to +\infty$. It is interesting to see that the resistance is not too much affected by H apart from in the region near depth based $Fn = 1$. For the lift, some difference is manly at Fn_c.

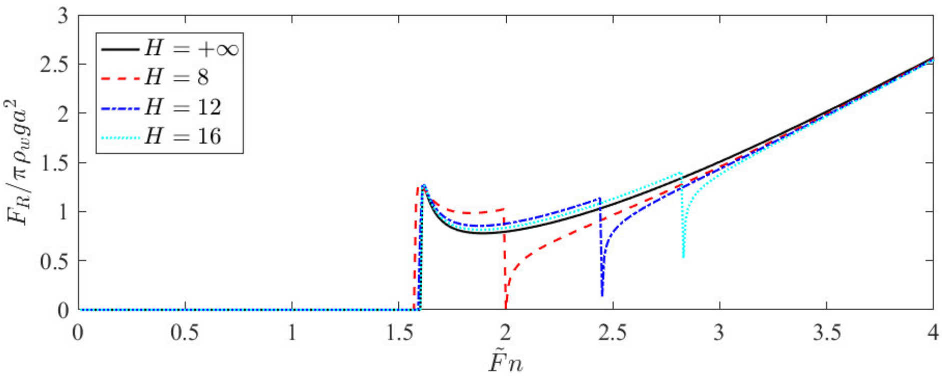

(a)

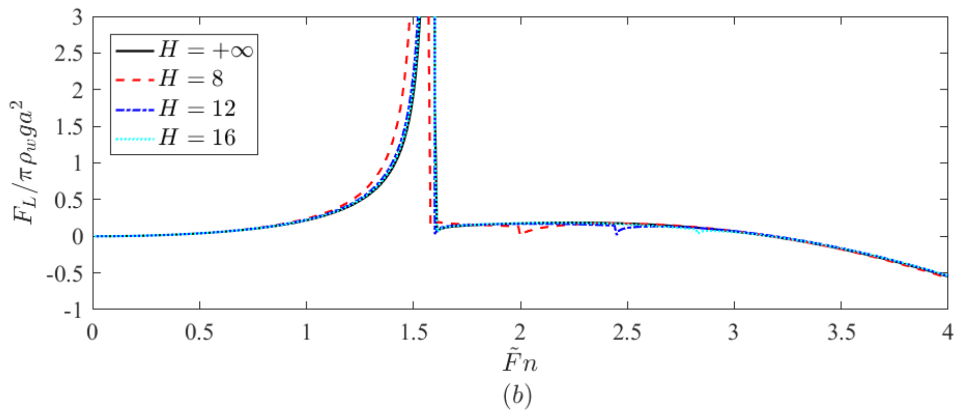

Fig. 6. Resistance (*a*) and lift (*b*) of a circular cylinder submerged below an ice sheet against submergence based $\tilde{F}n$ at different H. Solid lines: $H = +\infty$; dashed lines: $H = 8$; dash-dotted lines: $H = 12$; dotted lines: $H = 16$. ($a = 1$, $(x_0, z_0) = (0, -2)$, $h = 0.2$, $L = 72.9319$)

4.3. Deflection of the ice sheet

Computations are also carried out for the ice deflection η at different Froude number Fn. In figure 7 we show $\eta(x)$ plotted for $Fn < Fn_c$. It can be seen that there will be no wave propagating to infinity for all the four cases calculated. As can be observed, $\eta(x)$ is symmetric about $x = x_0$ due to fact that the last term, or the sine term, in (31) no longer exists at $Fn < Fn_c$. When Fn increases, the magnitude of the deflection above the cylinder increases. However, it remains to be a trough and reaches a very large value at $Fn = 0.775$ before $Fn_c = 0.7869$, which means that the gap between the ice sheet and cylinder will become very small. The large deflection of the ice sheet corresponds to the large lift, which can be seen in figure 5(*b*). As Fn further increase, the deflection above the cylinder drops rapidly and will become a peak as $Fn \to Fn_c$. Correspondingly, there is a rapid drop of the lift force. The ice deflection $\eta(x)$ within $Fn_c < Fn < 1$ is shown in figure 8. It can be observed that in such a case both sides of the body will have waves. Generally, the downstream ice deflection is larger than that in the upstream, which is more obvious for a larger Fn. As Fn approaches 1, k_2 tends to zero and its corresponding wavelength tends to infinity. In figure 9, $\eta(x)$ is plotted against x for $Fn > 1$. In such a case the longer wave at downstream disappears, but the shorter wave is still at upstream and its wavelength reduces as Fn increases. All these are consistent with the discussions in section 4.1 on the wave system in the far field through the dispersion equation.

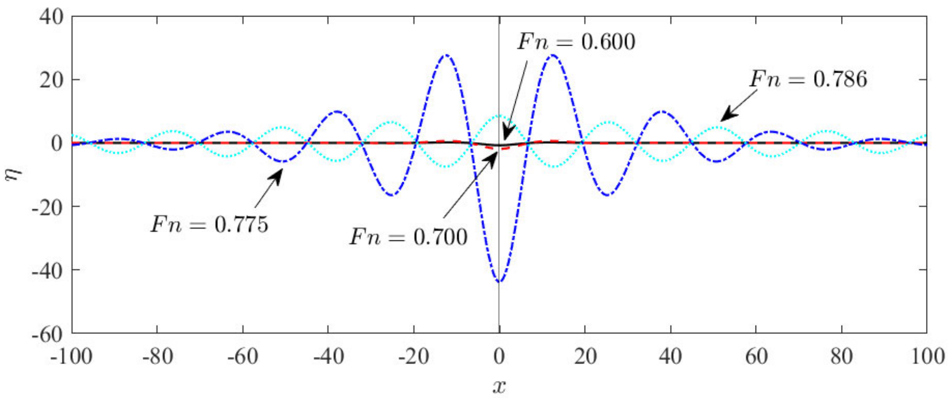

Fig. 7. Ice deflection $\eta(x)$ at different Froude number below Fn_c. Solid line: $Fn = 0.600$; dashed line: $Fn = 0.700$; dash-dotted line: $Fn = 0.775$; dotted line: $Fn = 0.786$. ($a = 1$, $(x_0, z_0) = (0, -2)$, $H = 8$, $h = 0.2$, $L = 72.9319$, $Fn_c = 0.7869$)

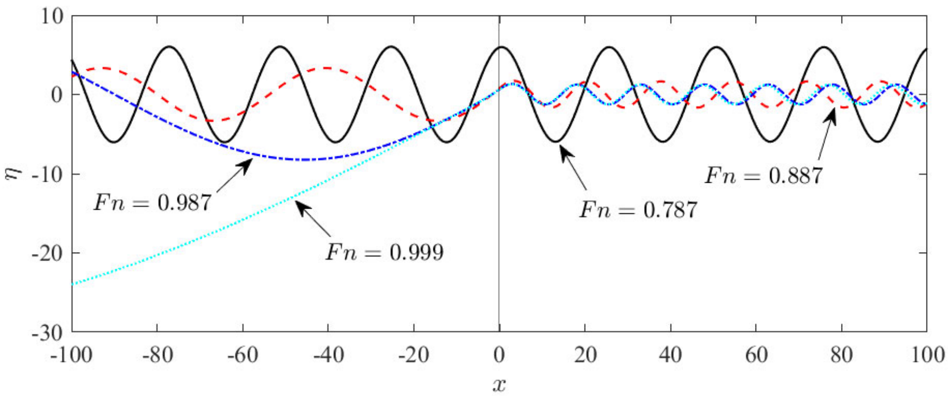

Fig. 8. Ice deflection $\eta(x)$ within the range of $Fn_c < Fn < 1$. Solid line: $Fn = 0.787$; dashed line: $Fn = 0.887$; dash-dotted line: $Fn = 0.987$; dotted line: $Fn = 0.999$. ($a = 1$, $(x_0, z_0) = (0, -2)$, $H = 8$, $h = 0.2$, $L = 72.9319$, $Fn_c = 0.7869$)

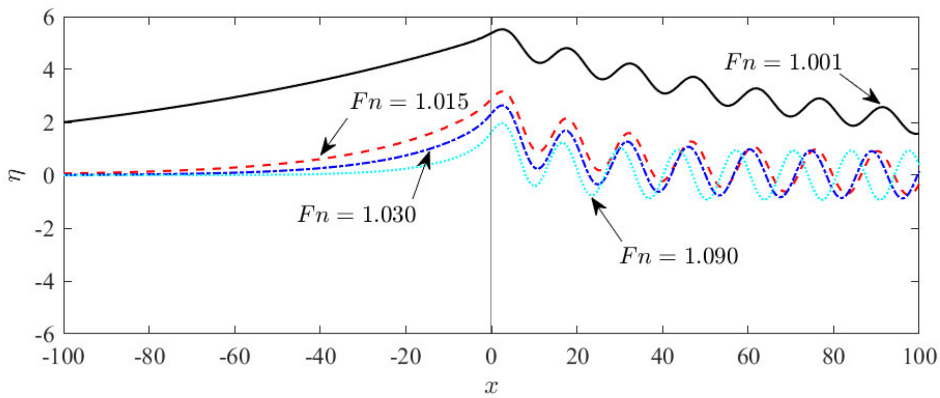

Fig. 9. Ice deflection $\eta(x)$ for $1 < Fn$. Solid line: $Fn = 1.001$; dashed line: $Fn = 1.015$; dash-dotted line: $Fn = 1.030$; dotted line: $Fn = 1.090$. ($a = 1$, $(x_0, z_0) = (0, -2)$, $H = 8$, $h = 0.2$, $L = 72.9319$, $Fn_c = 0.7869$)

5. Conclusions

The problem of a uniform current interacting with a circular cylinder submerged below an ice sheet of infinite extent has been solved. The ice sheet is modelled by a thin elastic plate floating on the water surface, and the fluid flow is described through the linearized velocity potential theory. The Green function satisfying all the boundary conditions apart from that on the body surface is derived by Fourier transform, through which the potentials due to multipoles are further obtained.

From the dispersion equation of finite water depth, it is found that there is a critical water depth Froude number Fn_c which depends on the properties of the ice sheet. When $Fn < Fn_c$ there will be no wave; when $Fn_c < Fn < 1$ there will be two waves, and the one with group velocity larger than current speed will travel at upstream, while the one with smaller group velocity will travel downstream. When $Fn > 1$, the downstream wave will disappear, while the upstream wave will be still there. This is similar to that noticed in related problem and different from that for open water. When the water depth tends to infinity, similar critical current speed also exists. However beyond the critical speed, there will be always two waves, one on each side of the body.

The results for ice sheet with different thicknesses show that the resistance generally increases with the ice thickness within the range calculated. The resistance will increase rapidly from zero when Fn becomes from $Fn < Fn_c$ to $Fn > Fn_c$. While the lift increases with Fn and will reach a large peak before Fn_c. As Fn further increases, the lift drops rapidly to a normal level and is mainly negative. Another rapid change of the resistance and lift occurs at $Fn = 1$.

The curve of the ice deflection shows that when $Fn < Fn_c$ the deflection is confined near to the cylinder and is symmetric. The deflection above the cylinder is a trough and its magnitude increases with Fn. It will reach a large value before Fn_c, and after that it will drops rapidly and even to become a peak. When $Fn > Fn_c$, the ice sheet on both sides of the cylinder will be in a wave form towards to infinity, and generally the magnitude of the deflection in the downstream is larger than that in the upstream. As $Fn > 1$, the deflection in the far downstream disappears while that in the upstream still exists.

The solution procedure can be further extended to the ice sheet with imperfections, e.g. fully detached or connected cracks. The Green function can also be used with the boundary element method for a body with arbitrary shape on the basis of the velocity potential flow theory.

Acknowledgement

This work is supported by Lloyd's Register Foundation through the joint centre involving University College London, Shanghai Jiaotong University and Harbin Engineering University, to which the authors are most grateful. Lloyd's Register Foundation helps to protect life and property by supporting engineering-related education, public engagement, and the application of research. This work is also supported by the National Natural Science Foundation of China (Grant No. 51879123 and 51709131)

References

Barrett, M.D., Squire, V.A., 1996. Ice-coupled wave propagation across an abrupt change in ice rigidity, density, or thickness. Journal of Geophysical Research Oceans 101, 20825-20832.

Chung, H., Linton, C.M., 2005. Reflection and transmission of waves across a gap between two semi-infinite elastic plates on water. Quarterly Journal of Mechanics and Applied Mathematics 58, 1-15.

Das, D., Mandal, B.N., 2006. Oblique wave scattering by a circular cylinder submerged beneath an ice-cover. International Journal of Engineering Science 44, 166-179.

Evans, D.V., Porter, R., 2003. Wave scattering by narrow cracks in ice sheets floating on water of finite depth. Journal of Fluid Mechanics 484, 143-165.

Fox, C., Squire, V.A., 1990. Reflection and transmission characteristics at the edge of shore fast sea ice. Journal of Geophysical Research Oceans 95, 11629–11639.

Grue, J., Palm, E., 1985. Wave radiation and wave diffraction from a submerged body in a uniform current. Journal of Fluid Mechanics 151, 257-278.

Li, Z.F., Shi, Y.Y., Wu, G.X., 2017a. Interaction of wave with a body floating on a wide polynya. Physics of Fluids 29, 097104.

Li, Z.F., Shi, Y.Y., Wu, G.X., 2017b. Large amplitude motions of a submerged circular cylinder in water with an ice cover. European Journal of Mechanics-B/Fluids 65, 141-159.

Li, Z.F., Shi, Y.Y., Wu, G.X., 2018a. Interaction of waves with a body floating on polynya between two semi-infinite ice sheets. Journal of Fluids and Structures 78, 86-108.

Li, Z.F., Wu, G.X., Ji, C.Y., 2018b. Interaction of wave with a body submerged below an ice sheet with multiple arbitrarily spaced cracks. Physics of Fluids 30, 057107.

Li, Z.F., Wu, G.X., Ji, C.Y., 2018c. Wave radiation and diffraction by a circular cylinder submerged below an ice sheet with a crack. Journal of Fluid Mechanics 845, 682-712.

Liu, Y., Li, H.J., 2016. Oblique flexural-gravity wave scattering by a submerged semi-circular ridge. Geophysical and Astrophysical Fluid Dynamics 110, 1-15.

Meylan, M.H., Squire, V.A., 1994. The response of ice floes to ocean waves. Journal of Geophysical Research Atmospheres 99, 891-900.

Mo, A., Palm, E., 1987. On radiated and scattered waves from a submerged elliptic cylinder in a uniform current. Journal of Ship Research 31, 23-33.

Porter, R., Evans, D.V., 2006. Scattering of flexural waves by multiple narrow cracks in ice sheets floating on water. Wave Motion 43, 425-443.

Porter, R., Evans, D.V., 2007. Diffraction of flexural waves by finite straight cracks in an elastic sheet over water. Journal of Fluids and Structures 23, 309-327.

Ren, K., Wu, G.X., Thomas, G.A., 2016. Wave excited motion of a body floating on water confined between two semi-infinite ice sheets. Physics of Fluids 28, 127101.

Robin, G.Q., 1963. Wave propagation through fields of pack ice. Philosophical Transactions of the Royal Society A255, 313-339.

Savin, A.A., Savin, A.S., 2012. Ice cover perturbation by a dipole in motion within a liquid. Fluid Dynamics 47, 139-146.

Squire, V.A., 2011. Past, present and impendent hydroelastic challenges in the polar and subpolar seas. Philosophical Transactions of the Royal Society A369, 2813-2831.

Squire, V.A., Dixon, T.W., 2000. An analytic model for wave propagation across a crack in an ice sheet. International Journal of Offshore and Polar Engineering 10, 173-176.

Squire, V.A., Dixon, T.W., 2001a. How a region of cracked sea ice affects ice-coupled wave propagation. Annals of Glaciology 33, 327-332.

Squire, V.A., Dixon, T.W., 2001b. On modelling an iceberg embedded in shore-fast sea ice. Journal of Engineering Mathematics 40, 211-226.

Squire, V.A., Hosking, R.J., Kerr, A.D., Langhorne, P.J., 1996. Moving loads on ice plates. Kluwer academic publishers, The Netherlands.

Squire, V.A., Robinson, W.H., Langhorne, P.J., Haskell, T.G., 1988. Vehicles and aircraft on floating ice. Nature 333, 159-161.

Sturova, I.V., 2013. Unsteady three-dimensional sources in deep water with an elastic cover and their applications. Journal of Fluid Mechanics 730, 392-418.

Sturova, I.V., 2014. Wave generation by an oscillating submerged cylinder in the presence of a floating semi-infinite elastic plate. Fluid Dynamics 49, 504-514.

Sturova, I.V., 2015a. The effect of a crack in an ice sheet on the hydrodynamic characteristics of a submerged oscillating cylinder. Journal of Applied Mathematics and Mechanics 79, 170-178.

Sturova, I.V., 2015b. Radiation of waves by a cylinder submerged in water with ice floe or polynya. Journal of Fluid Mechanics 784, 373-395.

Takizawa, T., 1985. Deflection of a floating sea ice sheet induced by a moving load. Cold Regions Science and Technology 11, 171-180.

Takizawa, T., 1988. Response of a floating sea ice sheet to a steadily moving load. Journal of Geophysical Research Oceans 93, 5100-5112.

Tkacheva, L.A., 2015. Oscillations of a cylindrical body submerged in a fluid with ice cover. Journal of Applied Mechanics and Technical Physics 56, 1084-1095.

Ursell, F., 1949. On the heaving motion of a circular cylinder on the surface of a fluid. Quarterly Journal of Mechanics and Applied Mathematics 2, 215-231.

Wehausen, J.V., Laitone, E.V., 1960. Surface waves, Handbuch des Physik. Springer Verlag, Berlin, pp. 446-778.

Wu, G.X., 1991. Hydrodynamic forces on a submerged cylinder advancing in water waves of finite depth. Journal of Fluid Mechanics 224, 645-659.

Wu, G.X., 1993. Hydrodynamic forces on a submerged circular cylinder undergoing large-amplitude motion. Journal of Fluid Mechanics 254, 41-58.

Wu, G.X., 1995. Radiation and diffraction by a submerged sphere advancing in water waves of finite depth. Proceedings of the Royal Society of London A448, 29-54.

Wu, G.X., 1998. Wave radiation and diffraction by a submerged sphere in a channel. Quarterly Journal of Mechanics and Applied Mathematics 51, 647-666.

Wu, G.X., Eatock Taylor, R., 1987a. The exciting force on a submerged spheriod in regular waves. Journal of Fluid Mechanics 182, 411-426.

Wu, G.X., Eatock Taylor, R., 1987b. Hydrodynamic forces on submerged oscillating cylinders at forward speed. Proceedings of the Royal Society of London A414, 149-170.